Applied Catalysis B: Environmental 95 (2010) 245–254

Contents lists available at ScienceDirect

Applied Catalysis B: Environmental

journal homepage: www.elsevier.com/locate/apcatb

NO_x photocatalytic degradation employing concrete pavement containing titanium dioxide

M.M. Ballari [a,*], M. Hunger [a,1], G. Hüsken [b,2], H.J.H. Brouwers [b,2]

[a] Department of Construction Management & Engineering, Faculty of Engineering Technology, University of Twente, P.O. Box 217, 7500 AE Enschede, The Netherlands
[b] Unit of Building Physics and Systems, Department of Architecture, Building and Planning, Eindhoven University of Technology, P.O. Box 513, 5600 MB Eindhoven, The Netherlands

ARTICLE INFO

Article history:
Received 1 October 2009
Received in revised form 22 December 2009
Accepted 7 January 2010
Available online 15 January 2010

Keywords:
Heterogeneous photocatalysis
Nitrogen oxides
Air purification
Concrete roads
NO and NO_2 kinetic model

ABSTRACT

In the present work the degradation of nitrogen oxides (NO_x) by concrete paving stones containing TiO_2 to be applied in road construction is studied. A kinetic model is proposed to describe the photocatalytic reaction of NO_x (combining the degradation of NO and the appearance and disappearance of NO_2) in a standard laminar flow photoreactor irradiated with UV lamps employing only NO as the contaminant source. In addition, the influences of several parameters that can affect the performance of these stones are investigated, such as NO inlet concentration, reactor height and flow rate. The kinetic parameters present in the NO and NO_2 reaction rate are estimated employing experimental data obtained in the photoreactor. The obtained model predictions employing the determined kinetic constants are in good agreement with the experimental results of NO and NO_2 concentration at the reactor outlet.

1. Introduction

Heterogeneous photocatalysis represents an emerging environmental control option for the efficient removal of chemical pollutants and it can be applied to water and air purification. This process involves a nano-solid semiconductor catalyst, regularly titanium dioxide (TiO_2), which is activated with ultraviolet light of the appropriate wavelength. For various reasons repetitively reported, titanium dioxide in the form of anatase has been the preferred choice due to its strong oxidizing power under UV irradiation, its chemical stability and the absence of toxicity [1]. These reactions are very attractive for treating pollution problems because: (1) in the vast majority of the cases transform pollutants into innocuous products [2–4] and (2) have very low selectivity, thus permitting the treatment of a wide range of contaminants.

Nitrogen oxides (NO_x) are the generic term for a group of highly reactive gases, most of them emitted in air in the form of nitric oxide (NO) and nitrogen dioxide (NO_2). Nitrogen oxides are for instance formed when fuel is burned at high temperatures, as it is the case in combustion processes in automobiles. NO_x causes a wide variety of health and environmental impacts, like the formation of tropospheric ozone and urban smog through photochemical reactions with hydrocarbons. Furthermore, NO_x together with SO_x (sulfur dioxide and sulfur trioxide) is the major contributor to the "acid rain", one of the most serious environmental problems across the world. Thus, NO_x emission is a focus of environmental regulations, especially in the ozone non-attainment areas.

The European Union (EU) has taken important steps over the past decade leading to a decrease in the emissions to air and water of a number of pollutants. One of its directives (1999/30/EC) [5] establishes limit values for concentrations of sulfur dioxide, nitrogen dioxide and oxides of nitrogen, particulate matter and lead in ambient air. Some of the pollutant emissions have since become more or less manageable; however particulates, NO_x and smog are still problematic.

To date, a number of researchers have investigated the dynamics of the photocatalysis of nitrogen oxides. While some of the NO_x control methodology is to reduce NO_x back to N_2 [6], another approach is to oxidize NO to NO_2 and HNO_3 along the general direction of nitrogen fixation. Photocatalytic oxidation (PCO) of NO_x offers the following distinctive advantages: (1) no extra reactants required and (2) NO_x recycled or recovered as nitric acid, a potential raw material for fertilizers. In 1994, Japanese researchers reported the photodegradation of NO_x in the ambient atmosphere, using TiO_2 as the photocatalyst [7]. Hashimoto et al. [8] reported the photocatalytic reaction of NO with TiO_2 and zeolite to remove NO_x in the atmosphere. Dalton et al. [9] investigated the NO_x absorbate reaction at the TiO_2 substrate surface. Ichiura et al. [10] studied the photocatalytic oxidation of nitrogen oxides over

* Corresponding author. Tel.: +31 0 53 489 4836; fax: +31 0 53 489 2511.
E-mail addresses: M.Ballari@ctw.utwente.nl, M.Ballari@tue.nl (M.M. Ballari).
[1] Tel.: +31 0 53 489 4836; fax: +31 0 53 489 2511.
[2] Tel.: +31 40 2472930; fax: +31 40 2438595.

0926-3373/$ – see front matter © 2010 Elsevier B.V. All rights reserved.
doi:10.1016/j.apcatb.2010.01.002

Nomenclature

a_v	active area per unit reactor volume [$dm^2\ dm^{-3}$]
A	area [dm^2]
B	reactor width [dm]
C	molar concentration [$mol\ dm^{-3}$]
D_h	hydraulic diameter [dm]
E	radiative flux [$W\ m^{-2}$]
H	reactor height [dm]
k	reaction rate constant [$mol\ dm^{-2}\ min^{-1}$]
K	adsorption equilibrium constant [$dm^3\ mol^{-1}$]
L	reactor length [dm]
L_d	length for a fully developed parabolic velocity profile [dm]
N	number
Q	flow rate [$l\ min^{-1}$]
r	superficial reaction rate [$mg\ dm^{-2}\ min^{-1}$]
Re	Reynolds number
t	time [min]
v	velocity [$dm\ min^{-1}$]
V	volume [dm^3]
x	Cartesian coordinate [dm]

Greeks letters

η	dynamic viscosity [$g\ m^{-1}\ s^{-1}$]
ρ	density [$g\ m^{-3}$]
υ	kinematic viscosity [$m^2\ s^{-1}$]

Subscripts

act	active
ads	adsorbed
air	air
in	inlet condition
NO	nitric oxide
NO_2	nitrogen dioxide
out	outlet condition
reactor	reactor

titanium dioxide sheets containing metal compounds. In addition, Devahasdin et al. [11] studied the transient behavior and reaction kinetics of the NO photocatalytic degradation, and discussed the feasibility of nitrogen fixation in the flue gas treatment with photocatalytic oxidation. Lin et al. [12] examined the photocatalytic degradation of nitrogen oxides over titania-based photocatalyst illuminated by ultraviolet and visible light. Shelimov et al. [13] analyzed the efficiency of TiO_2 dispersed over alumina support in the photocatalytic removal of NO_x.

The development of innovative materials that can be easily applied on structures, with both de-soiling and de-polluting properties, is a significant step towards improvements of air quality. The use of TiO_2 photocatalyst in combination with cementitious and other construction materials has shown a favorable effect in the removal of air pollutants [14]. In recent years, a wide number of laboratory scale tests have been performed, under different experimental conditions, in order to evaluate the NO_x degradation properties of TiO_2 photocatalytic materials [15–20]. The application of photocatalytic materials is protected by several patents [21–25].

However, few of the studies mentioned above have considered the reaction kinetics of the NO and NO_2 together as a series-parallel or consecutive–competitive reaction and none of them have proposed a kinetic expression for the appearance–disappearance of NO_2. Only reaction rate expressions for the degradation of NO were proposed, which sometime involve the effect of the NO_2 concentration. For instance, Devahasdin et al. [11] proposed a NO reaction rate equation in function of the NO_2 concentration. On the other hand, Hashimoto et al. [8] performed an active site balance for NO and NO_2 and proposed two expressions corresponding with the equilibrium adsorption concentrations for both species.

In the present work, the degradation of NO_x compounds employing commercial concrete paving stones with TiO_2 to be applied in road construction is studied experimentally and theoretically. The experiments were carried out in a photoreactor designed according to standard ISO 22197-1 [26] to assess these kinds of photocatalytic materials employing NO as the pollutant source. Furthermore, a kinetic model is proposed to describe the photocatalytic oxidation of NO_x (NO and NO_2). A reaction rate expression for the oxidation of NO as well as for the appearance and disappearance of NO_2 are postulated and the kinetic parameters are determined employing the experimental data. In addition, the influence of several parameters that can affect the performance of these stones, such as NO inlet concentration, reactor height and flow rate is studied. The relative humidity, temperature and irradiance were kept constant during this study. Finally, the model predictions with the estimated kinetic constants are compared with the experimental results tielding a good agreement between them.

2. Experimental setup and measurements

The standard ISO 22197-1 [26] serves as a sound basis for measurements, its recommendations were largely followed for the practical conduction of the present study. In fact, this standard holds for advanced technical fine ceramics but it satisfies the needs for measurements on concrete specimen as well.

The applied apparatus is composed of a reactor cell housing the sample, a suitable light source, a NO_x analyzer, and an appropriate gas supply (Fig. 1).

2.1. Reactor

The core of the experimental setup is a gas reactor allowing a planar sample of the size 100 mm × 200 mm to be embedded. The schematic representation of the gas reactor is given in Fig. 2.

Furthermore, the reactor is made from materials which are non-adsorbing to the applied gas and can withstand UV light of high radiation intensity. On top the reactor is tightly closed with a glass pane made from borosilicate, allowing the UV-radiation to pass through with almost no resistance. Within the reactor the planar surface of the specimen is fixed parallel to the covering glass, leaving an alterable slit height H (most commonly 3 mm) for the gas to pass through. The active sample area used for degradation was, deviating from the standard, enlarged from 49.5 mm ± 0.5 mm in width and 99.5 mm ± 0.5 mm in length to B = 100 mm and L = 200 mm (with similar tolerance), which better complies with standard paving stone dimensions. By means of profiles and seals, the sample gas only passes the reactor through the slit between sample surface in longitudinal direction and the glass cover. All structural parts inside the box are designed to enable laminar flow of the gas along the sample surface and to prevent turbulences.

2.2. Light source

The applied light source is composed of three fluorescent tubes (Philips CLEO Compact) of each 25 W, emitting a high-concentrat-

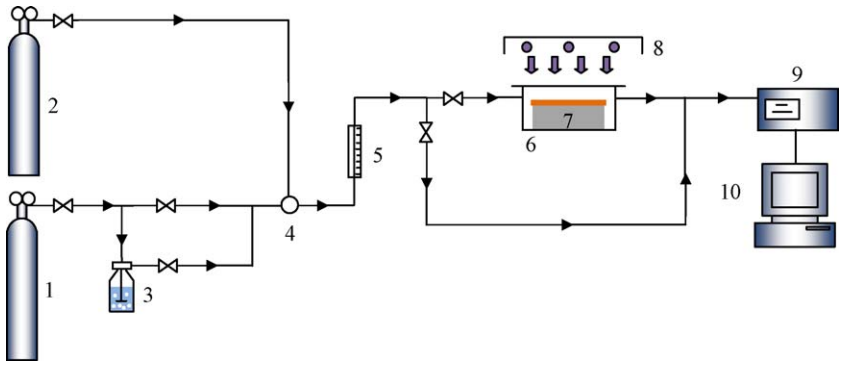

Fig. 1. Schematic representation of the experimental setup. (1) Synthetic air. (2) NO source. (3) Gas-washing bottle. (4) Temperature and relative humidity sensor. (5) Flow controller. (6) Gas photoreactor. (7) Paving stone sample. (8) Light source. (9) NO_x analyzer. (10) Computer.

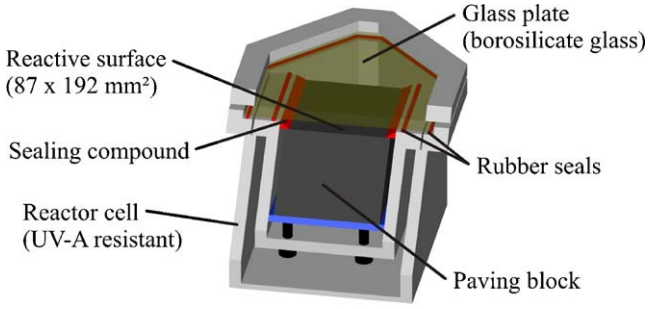

Fig. 2. Schematic diagram of the gas photoreactor.

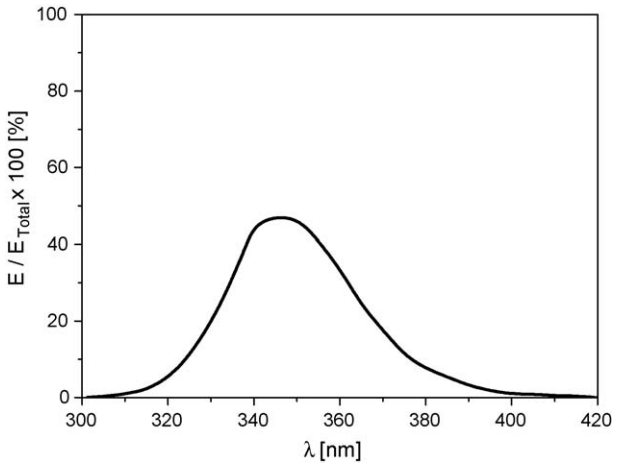

Fig. 3. Spectral distribution of the relative emission of the employed lamps.

ed UV-A radiation in the range of 300–400 nm with maximum intensity at about 345 nm (Fig. 3). Due to the narrow range in wavelength, an addition of a filter was not necessary. A warming of the reactor by the light source is not expected due to the spatial separation of light source and reactor, and a cooling of the lamp by means of fans. All fluorescent tubes can be adjusted in irradiance. With the help of a calibrated UV-A radiometer the irradiance is adjusted to 10 W m^{-2} at the sample surface. A lead time of about 15 min has to be considered for fluorescent tubes till a stable UV-A radiation is approached. The UV-A irradiance profile within the test setup and surrounding the reactor box can be observed in Fig. 4.

2.3. Testing gas supply and gas types

For the conduction of the experiment, two different types of gas, filled in standard gas cylinders, are necessary. First, the model contaminant is discussed. For the pollution of the sample surfaces, nitric oxide (NO) is employed. The used gas is composed of 50 ppmv NO which is stabilized in nitrogen (N_2). As the concentration of gas, finally applied to the sample, is adjusted to 1 ppmv, only small quantities of this gas are required. As transport fluid synthetic air, being composed of 20.5 vol.% of oxygen (O_2) and 79.5 vol.% of nitrogen, is used.

Since the gas cylinders are under high pressure, the gas needs to pass a pressure reducing valve before entering the system. Here, pressure is first reduced to 0.3 bar. Before the two gas flows are merged, the model contaminant has to pass a high precision valve in order to adjust a pollution of 1 ppmv NO to the sample. The NO concentration can be monitored with the NO analyzer, connected

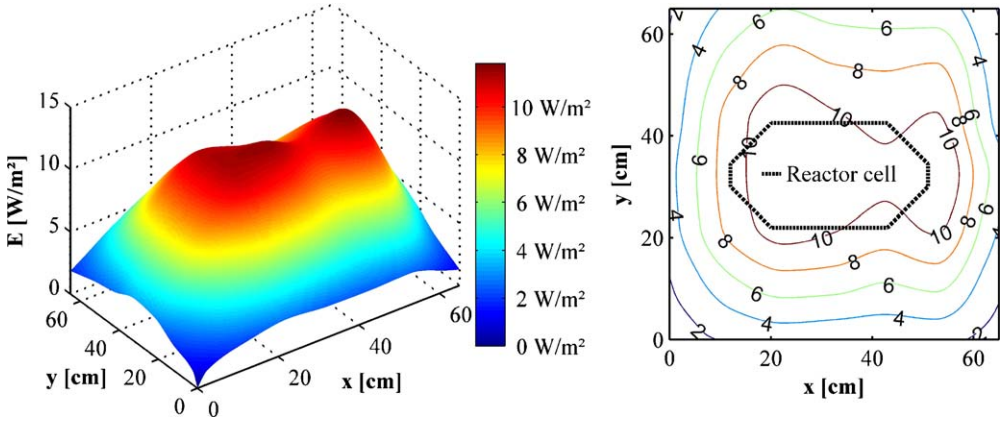

Fig. 4. Distribution of UV-A irradiance within the test setup (left) and placement of the reactor box (right).

to the outlet of the reactor box. Furthermore, the synthetic air is conveyed through a gas-washing bottle, filled with demineralized water, in order to keep the relative humidity of the supplied gas constant at 50%. Using a split gas flow, with one line passing a valve before the gas-washing bottle, the desired humidity can be adjusted. Behind these two stages both gas flows, polluted and transport fluid, are mixed. With the help of a flow controller a volume flow of $Q = 3\ \mathrm{l\ min^{-1}}$ is adjusted. The Reynolds number of the flow reads:

$$Re = \frac{\upsilon_{air} D_h \rho_{air}}{\eta_{air}} = \frac{2\upsilon_{air} H \rho_{air}}{\eta_{air}} = \frac{2Q}{B\upsilon_{air}} \quad (1)$$

D_h is the hydraulic diameter of the considered channel, defined as four time the cross-sectional area divided by the perimeter, for the slit considered here, $D_h = 2H$. Substituting $Q = 3\ \mathrm{l\ min^{-1}}$, $B = 100\ \mathrm{mm}$ and $\upsilon_{air} = 1.54 \times 10^{-5}\ \mathrm{m^2\ s^{-1}}$ (1 bar, 20 °C) yields $Re \approx 65$. Considering $H = 3$ mm, the mean air velocity υ_{air} is $0.17\ \mathrm{m\ s^{-1}}$ along the sample surface.

This low Reynolds number implies that the flow is laminar. A fully developed parabolic velocity profile will be developed at $L_d = 0.05\ Re\ 2H$, so here $L_d \approx 20$ mm, i.e. only at the first 10% of the slit length there are entrance effects, during the remaining 90% there is a fully developed laminar flow profile.

The gas, mixed and humidified this way, enters the reactor and is conveyed along the illuminated sample surface. At the opposite site of the reactor the gas leaves the chamber and is transported to a flue or outside with the help of an exhaust air duct. The NO_x analyzer samples the reacted gas from this exhaust line. An adequate dimensioning of the hose line and, possibly, the installation of non-return valves prevents from suction of leak air from outside via the hose line to the analyzer.

2.4. Analyzer

For the gas analysis a chemiluminescent NO_x analyzer is employed. The analyzer measures the NO_x and NO concentration in steps of 5 s while the corresponding NO_2 concentration is computed by the difference of the previous two. During the measurement the analyzer is constantly sampling gas with a rate of $0.8\ \mathrm{l\ min^{-1}}$. The detection limit of the employed analyzer is at about 0.5 ppbv.

2.5. The conduction of measurements

For the development of a reaction model and the herewith related experiments one sample, a paving stone, was used. This way differences in measurement results due to varying surface roughness or unequal distribution of catalyst can be neglected. The employed sample is a commercially available concrete paving stone whose photocatalytic properties were tested beforehand [27] and is a double layer stone with the upper layer being photocatalytically active. This upper layer was prepared mixing dry powders of normal concrete with TiO_2 powder before adding water to the mixture. Further information about the concrete recipe cannot be provided because it is confidential information of the manufacturing company.

In preparation of each measurement the sample surface is cleaned with demineralized water in order to remove fouling, contamination and potential reaction products due to a previous NO_x degradation. Subsequently, the sample is dried in a drying oven for 24 h. For the measurement, the sample is placed in the reaction chamber and with the help of an elastic sealing compound all gaps and joints are sealed that way that the fed air can only pass the reactor along the reactive sample surface. A metal sheet of the dimension 87 mm × 192 mm is employed as a template for the sealing. Therefore, the active sample surface is kept exactly identical for all measurements.

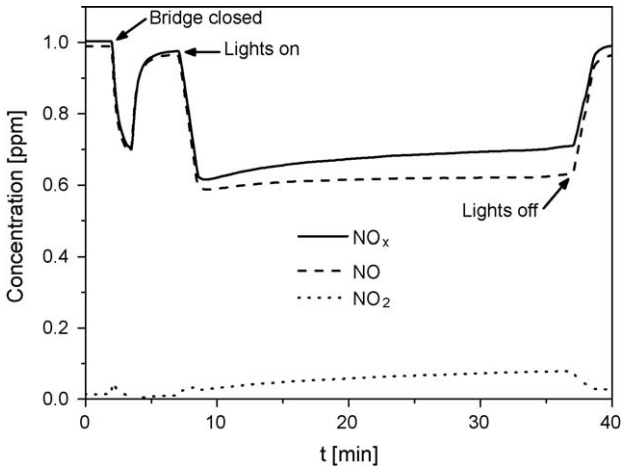

Fig. 5. Representative experimental result. $H = 3$ mm. $Q = 3$ l min^{-1}. $C_{NO,in} = 1.0$ ppm. 50% relative humidity. $E = 10\ \mathrm{W\ m^{-2}}$.

After assembling the sample the reactor is closed and the gas supply is started. The UV-A source is switched on as well in order to start the radiation stabilization, but the reactor stays covered to prevent first degradation. With the help of the controls the flow and relative humidity are now adjusted. The supplied NO concentration is adjusted to the desired inlet concentration, which is checked by the analyzer. When these conditions are stable the bridge is closed and the gas flows along the reactor. During this time the measured NO outlet concentration of the reactor decreases and then approaches again the original inlet concentration. This phenomenon describes the saturation of surface with NO as well as the non contaminated air removal from the reactor and has been found to be a function of flow velocity, inlet concentration and surface character of the sample. After this period of time, the cover sheet is removed to allow the UV-radiation passing through the glass. The degradation for the uncovered reactor lasts for 30 min, then the reactor is covered again and the data acquisition is continued for further 5 min. Within the last minutes of measurement the NO and NO_x concentrations return to the original scale. An example of a representative experiment result is shown in Fig. 5, where the different steps mentioned above can be observed.

In order to obtain sufficient data for the development of a reaction model, varying NO inlet concentrations of 0.1, 0.3, 0.5, and 1.0 ppmv were applied. Furthermore, for each inlet concentration the flow rate was varied by using flows of 3 and $5\ \mathrm{l\ min^{-1}}$. These different volumetric flows correspond to flow velocities of 0.167 and $0.278\ \mathrm{m\ s^{-1}}$ at the sample surface inside the reactor box. With these combinations a total number of 8 measurements were executed plus 4 repetitions under certain operation conditions (Table 1).

In addition, five more measurements with the above given flow rates but a fixed NO inlet concentration of 0.3 ppmv have been done. In doing so, the slit height in the reactor box was varied (2, 3 and 4 mm) for each flow rate. However, stable and measurable NO inlet concentration could not be achieved while applying a flow of $5\ \mathrm{l\ min^{-1}}$ and using a slit height of only 2 mm and this experiment was excluded.

2.6. Modelling

The photocatalytic oxidation mechanism of NO_x mixture is reported in many publications [7,9,11,13,17]. All of them proposed the NO decomposition to NO_2, and then NO_2 to NO_3H through the hydroxyl radical attack generated during the photocatalyst

Table 1
Experimental results of the photocatalytic NO degradation with an active concrete surface for different operating conditions.

Experiment #	Q l min^{-1}	H mm	$C_{NO,in}$ ppm	$C_{NO,out}$ ppm	$C_{NO_2,in}$ ppm	$C_{NO_2,out}$ ppm	NO_x conversion %
1	3	3	0.096	0.030	0.002	0.005	64.29
2	3	3	0.304	0.159	0.003	0.006	46.25
3	3	2	0.301	0.162	0.004	0.009	43.93
4	3	4	0.301	0.158	0.005	0.012	44.44
5	3	3	0.505	0.312	0.004	0.008	37.13
6	3	3	0.505	0.342	0.009	0.010	31.52
7	3	3	0.989	0.624	0.015	0.077	30.18
8	3	3	1.001	0.724	0.018	0.080	21.10
9	3	3	1.009	0.736	0.016	0.042	24.10
10	3	3	1.009	0.763	0.014	0.050	20.53
11	5	3	0.102	0.041	0.002	0.008	52.88
12	5	3	0.300	0.197	0.004	0.012	31.25
13	5	4	0.300	0.208	0.005	0.009	28.85
14	5	3	0.502	0.357	–	–	28.88
15	5	3	0.998	0.777	0.020	0.081	15.72

Table 2
Photocatalytic reaction mechanism of nitrogen oxides.

Reaction step								Constant
Activation	TiO_2	+	hv	→	h^+	+	e^-	Φ_λ
Absorption	H_2O_{gas}	+	Site	⇔	H_2O_{ads}			K_W
	O_{2gas}	+	Site	⇔	O_{2ads}			K_{O_2}
	NO_{gas}	+	Site	⇔	NO_{ads}			K_{NO}
	NO_{2gas}	+	Site	⇔	NO_{2ads}			K_{NO_2}
Hole trapping	H_2O_{ads}	+	h^+	→	$^\bullet OH$	+	H^+	k_1
Electron trapping	O_2	+	e^-	→	O_2^-			k_2
Hydroxyl attack	NO_{ads}	+	$^\bullet OH$	→	HNO_2			k_3
	HNO_2	+	$^\bullet OH$	→	NO_{2ads}	+	H_2O	k_4
	NO_{2ads}	+	$^\bullet OH$	→	HNO_3			k_5
Superoxide attack	NO_{ads}	+	O_2^-	→	NO_3^-			k_6
Recombination	h^+	+	e^-	→	Heat			k_7

activation stage. However, despite of these mechanisms being self consistent, in some of the reaction schemes additional reaction processes are proposed, like O_2^- interaction with NO to yield NO_3^- [13]. The scheme postulated in the present work is shown in Table 2 considering the studies mentioned above.

The kinetic expression proposed for the NO degradation reaction rate is the corresponding to the Langmuir–Hinshelwood model [11,17,28] which is widely employed for the photocatalytic degradation of a number of contaminants [29–31]. Nevertheless, only few times the photocatalytic kinetic model includes the reaction dependence with other reactants and/or intermediates concentrations (in this case NO_2) [11]. Moreover, the reaction rate should be expressed as a superficial rate for a gas-solid heterogeneous system [18,19,32–35]. Following this model, applied to a heterogeneous reaction, the Langmuir–Hinshelwood kinetic model for NO disappearance rate and NO_2 appearance/disappearance rate for irreversible reactions, per unit area of active surface and for constants relative humidity and irradiance reads:

$$r_{NO} = -r_3 - r_6 = -\frac{(k_3 + k_6)K_{NO}C_{NO}}{1 + K_{NO}C_{NO} + K_{NO_2}C_{NO_2}} \quad (2)$$

$$r_{NO_2} = -r_5 + r_4 = -r_5 + r_3 = -\frac{k_5 K_{NO_2}C_{NO_2}}{1 + K_{NO}C_{NO} + K_{NO_2}C_{NO_2}} + \frac{k_3 K_{NO}C_{NO}}{1 + K_{NO}C_{NO} + K_{NO_2}C_{NO_2}} \quad (3)$$

where r_3, r_4, r_5 and r_6 are the superficial reaction rates (mol dm^{-2} min^{-1}) of the corresponding stage as Table 2 shows. C_{NO} and C_{NO_2} are the corresponding molar concentration (mol dm^{-3}) of NO and NO_2 (which are related to the NO and NO_2 concentrations in ppm through the air volume under normal condition of 1 bar and 20 °C). k_3, k_5 and k_6 are the corresponding reaction rate constants (mol dm^{-2} min^{-1}) for NO and NO_2. K_{NO} and K_{NO_2} are the adsorption equilibrium constant (dm^3 mol^{-1}) for NO and NO_2 respectively, assuming that these species compete for the same active sites.

Here, the adopted hypothesis in the NO_2 reaction rate expression is $r_4 = r_3$, that corresponds to the kinetic or micro steady state for the NO_2H specie, that was found in very low concentration [11].

In addition, other assumptions can be imposed after doing the parameters optimization as shown in next section. A small value of k_6 (8 order of magnitude smaller than k_3) was obtained employing Eqs. (2) and (3) in the parameters optimization tool. Therefore, a simpler kinetic model (with less kinetic parameters) can be achieved by taking into account the hydroxyl attack as the main NO_x degradation mechanism, i.e. the same as Devahasdin et al. [11] have proposed:

$$r_{NO} = -r_3 = -\frac{k_3 K_{NO}C_{NO}}{1 + K_{NO}C_{NO} + K_{NO_2}C_{NO_2}} \quad (4)$$

$$r_{NO_2} = -r_5 + r_4 = -r_5 + r_3 = -\frac{k_5 K_{NO_2}C_{NO_2}}{1 + K_{NO}C_{NO} + K_{NO_2}C_{NO_2}} + \frac{k_3 K_{NO}C_{NO}}{1 + K_{NO}C_{NO} + K_{NO_2}C_{NO_2}} \quad (5)$$

Since Hunger et al. [28] have found that this kind of system employing a photocatalytic concrete stone in a flow reactor is not controlled by the mass transport, a plug flow reactor model can be

assumed for the NO and NO_2 balance equations:

$$v_{air}\frac{dC_{NO}}{dx} = a_v r_{NO} \quad (6)$$

$$v_{air}\frac{dC_{NO_2}}{dx} = a_v r_{NO_2} \quad (7)$$

where a_v is the active surface area per unit reactor volume:

$$a_v = \frac{A_{act}}{V_{reactor}} \cong \frac{1}{H}[=]\frac{dm^2_{act}}{dm^3_{reactor}} \quad (8)$$

and with the following inlet conditions:

$$C_{NO}(x=0) = C_{NO,in} \quad (9)$$

$$C_{NO_2}(x=0) = C_{NO_2,in} \quad (10)$$

Replacing the kinetic equations (Eqs. (4) and (5)) in the corresponding mass balances (Eqs. (6) and (7)):

$$v_{air}\frac{dC_{NO}}{dx} = -a_v\frac{k_3K_{NO}C_{NO}}{1+K_{NO}C_{NO}+K_{NO_2}C_{NO_2}} \quad (11)$$

$$v_{air}\frac{dC_{NO_2}}{dx} = a_v\left(-\frac{k_5K_{NO_2}C_{NO_2}}{1+K_{NO}C_{NO}+K_{NO_2}C_{NO_2}}+\frac{k_3K_{NO}C_{NO}}{1+K_{NO}C_{NO}+K_{NO_2}C_{NO_2}}\right) \quad (12)$$

In addition to the study performed by Hunger et al. [28], the validity of the above mass balance model was assessed using a 2-Dimensional CFD simulation (Comsol Multiphysics). Even though concentration gradients along the vertical direction of the reactor were found, the outlet concentration predicted by the CFD simulations differs in less than 8% from the 1-dimensional plug flow model. Therefore, the 1D mass balance is a suitable approximation for the current flow reactor, despite of the above mentioned laminar flow regime. The simulation results employing the CFD tool will be presented in a forthcoming paper.

3. Resulting solutions

3.1. Approximate solution

Both obtained differential equations (Eqs. (11) and (12)) are connected and they can be only solved numerically employing for instance the Euler method, which will be described in the next section. However, some approximations can be considered in order to get an analytical solution of the mass balances. By dividing Eq. (12) by Eq. (11), a differential equation of NO_2 concentration in function of NO concentration is obtained:

$$\frac{dC_{NO_2}}{dC_{NO}} = \frac{k_5K_{NO_2}C_{NO_2}}{k_3K_{NO}C_{NO}} - 1 \quad (13)$$

With the following boundary condition:

$$C_{NO_2}(C_{NO} = C_{NO,in}) = C_{NO_2,in} \quad (14)$$

If $k_5K_{NO_2} \neq k_3K_{NO}$, the solution is:

$$C_{NO_2} = \left(\frac{C_{NO,in}}{1-(k_5K_{NO_2}/k_3K_{NO})}+C_{NO_2,in}\right)\times\left(\frac{C_{NO}}{C_{NO,in}}\right)^{k_5K_{NO_2}/k_3K_{NO}} - \frac{C_{NO}}{1-(k_5K_{NO_2}/k_3K_{NO})} \quad (15)$$

Considering that $C_{NO,in}/C_{NO}(x>0) > 1$, this expression can be simplified if $(k_5K_{NO_2}/k_3K_{NO}) > 1$ and if $C_{NO_2,in} \approx 0$, obtaining:

$$C_{NO_2} = \frac{C_{NO}}{(k'_5K'_{NO_2}/k'_3K'_{NO})-1} \quad (16)$$

where k'_5, K'_{NO_2}, k'_3 and K'_{NO} denote the kinetic parameters of the approximate model.

In cases where the only fed contaminant is NO, which is the case following the standard ISO 22197-1 [26], $C_{NO_2}(x=0) = 0$ and $C_{NO_2} \ll C_{NO}$ can be assumed [28]. Hence, $1 + K_{NO}C_{NO} \gg K_{NO_2}C_{NO_2}$ and the NO balance can be written as:

$$v_{air}\frac{dC_{NO}}{dx} = -a_v\frac{k'_3K'_{NO}C_{NO}}{1+K'_{NO}C_{NO}} \quad (17)$$

with

$$C_{NO}(x=0) = C_{NO,in} \quad (18)$$

Integration of Eq. (17) and using the boundary condition (Eq. (18)) yields:

$$\frac{1}{k'_3}+\frac{1}{k'_3K'_{NO}}\frac{\ln(C_{NO,in}/C_{NO,out})}{(C_{NO,in}/C_{NO,out})} = \frac{a_vL}{v_{air}(C_{NO,in}-C_{NO,out})} = \frac{BL}{Q(C_{g,in}-C_{g,out})} \quad (19)$$

with $Q = v_{air}BH$ and $C_{NO,out} = C_{NO}(x = L)$. This equation was also obtained and successfully applied by Hunger et al. [28], who considered an NO balance only.

Thus employing Eqs. (16) and (19) plus the experimental data under different operating conditions, the kinetic parameters for the NO and NO_2 photocatalytic reaction can be obtained.

In Fig. 6, $y = BL/Q(C_{NO,in} - C_{NO,out})$ is set out vs. $x = \ln(C_{NO,in}/C_{NO,out})/(C_{NO,in} - C_{NO,out})$ (according to Eq. (19)), and the data fit with the line $y = (0.336\ min\ dm^{-1})x + 4.182 \times 10^7\ min\ dm^2\ mol^{-1}$. The intersection with the ordinate corresponds to $1/k'_3$, so that $k'_3 = 0.239 \times 10^{-7}\ mol\ dm^{-2}\ min^{-1}$, and the slope to $1/k'_3K'_{NO}$, so that $K'_{NO} = 12.443 \times 10^7\ dm^3\ mol^{-1}$. The regression results are shown in Table 3 as well, including the standard errors and the 95% confidence intervals of the parameters. These values of $a_vk'_3$ and K'_{NO} are in line with those values k and K_d respectively presented by Hunger et al. [28].

At this time, from the NO kinetic parameters estimated with Eq. (19) and from Eq. (16), the kinetic information for the NO_2 photocatalytic reaction can be determined. Fig. 7 shows the NO_2 outlet concentration ($C_{NO_2,out}$) in function of NO outlet concentration ($C_{NO,out}$) and the linear regression result with the ordinate intercept equal to zero. The slope obtained is $1/((k'_5K'_{NO_2}/k'_3K'_{NO}) - 1) = 0.084$ and therefore $k'_5K'_{NO_2} = 38.41\ dm\ min^{-1}$ (Table 4). Considering Eq. (16), this result indicates that during the standard experiments the NO_2 at the outlet is about 8.4% of the NO

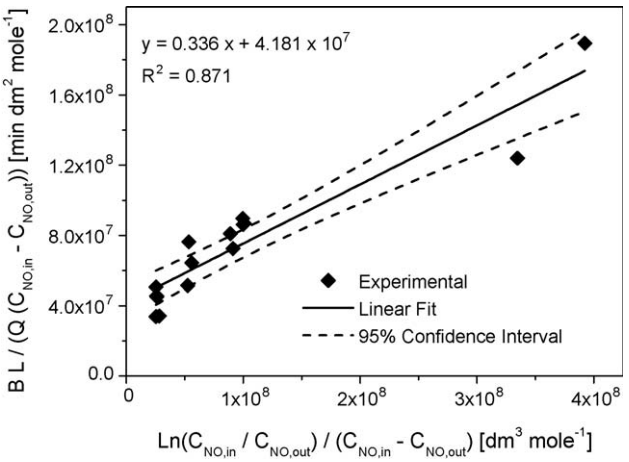

Fig. 6. Linear regression employing the approximate solution of the NO differential mass balance.

Table 3
Linear regression results employing the approximate solution of the NO differential mass balance.

Parameter	Value	Standard error	Lower 95% confidence interval	Upper 95% confidence interval
$\frac{1}{k'_3 K'_{NO}}$ (min dm^{-1})	0.336	0.034	0.262	0.410
$\frac{1}{k'_3}$ (min dm^2 mol^{-1})	4.18×10^7	0.51×10^7	3.09×10^7	5.27×10^7
k'_3 (mol dm^{-2} min^{-1})	0.239×10^{-7}	0.029×10^{-7}	0.177×10^{-7}	0.302×10^{-7}
K'_{NO} (dm^3 mol^{-1})	12.44×10^7	2.76×10^7	6.46×10^7	18.43×10^7
R^2	0.871			
N (*)	15			

(*) Number of data.

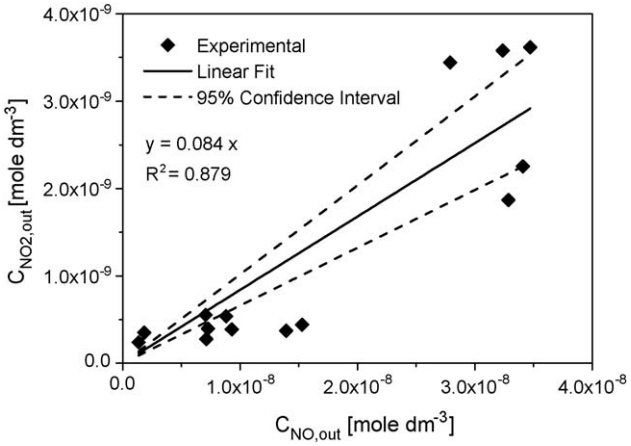

Fig. 7. Linear regression employing the approximate solution of the differential equation of NO_2 concentration in function of NO concentration.

concentration at the outlet, notwithstanding that NO_2 at the entrance is zero.

3.2. Complete solution

To solve the coupled NO and NO_2 mass balance with the complete kinetic expression, a discretization of the differential equations (Eqs. (11) and (12)) can be applied (Euler method):

$$v_{air}\frac{C_{NO,i+1}-C_{NO,i}}{x_{i+1}-x_i} = -a_v \frac{k_3 K_{NO} C_{NO,i}}{1+K_{NO}C_{NO,i}+K_{NO_2}C_{NO_2,i}} \quad (20)$$

$$v_{air}\frac{C_{NO_2,i+1}-C_{NO_2,i}}{x_{i+1}-x_i} = a_v\left(-\frac{k_5 K_{NO_2} C_{NO_2,i}}{1+K_{NO}C_{NO,i}+K_{NO_2}C_{NO_2,i}} + \frac{k_3 K_{NO} C_{NO,i}}{1+K_{NO}C_{NO,i}+K_{NO_2}C_{NO_2,i}}\right) \quad (21)$$

So

$$C_{NO,i+1} = -a_v\left(\frac{k_3 K_{NO} C_{NO,i}}{1+K_{NO}C_{NO,i}+K_{NO_2}C_{NO_2,i}}\right)\frac{x_{i+1}-x_i}{v_{air}} + C_{NO,i} \quad (22)$$

Table 5
Non-linear parameters optimization employing the Excel Solver tool and the numerical solution of the NO and NO_2 differential mass balance performing a forward discretization.

Parameter	Value	95% confidence interval
k_3 (mol dm^{-2} min^{-1})	0.47×10^{-7}	0.01×10^{-7}
K_{NO} (dm^3 mol^{-1})	3.40×10^7	0.08×10^7
k_5 (mol dm^{-2} min^{-1})	15.38×10^{-7}	0.02×10^{-7}
K_{NO_2} (dm^3 mol^{-1})	1.24×10^7	0.13×10^7
$k_5 K_{NO_2}$ (dm min^{-1})	19.07	2.10
$\frac{k_5 K_{NO_2}}{k_3 K_{NO}}$	11.93	1.71
N (*)	29	

$$C_{NO_2,i+1} = a_v\left(-\frac{k_5 K_{NO_2} C_{NO_2,i}}{1+K_{NO}C_{NO,i}+K_{NO_2}C_{NO_2,i}} + \frac{k_3 K_{NO} C_{NO,i}}{1+K_{NO}C_{NO,i}+K_{NO_2}C_{NO_2,i}}\right)\frac{x_{i+1}-x_i}{v_{air}} + C_{NO_2,i} \quad (23)$$

where $i = 1 \ldots N$ and $L_R = (x_{i+1} - x_i)(N-1)$.

The optimum values of all kinetic parameters present in Eqs. (22) and (23) were obtained employing the Excel (Microsoft) "solver" tool. These results and the 95% confidence intervals are shown in Table 5. The estimated absorption constants for NO and NO_2 are in fairly agreement with those values calculated by Hashimoto et al. [8] employing titania-zeolite composite catalyst ($K_{NO} = 1.17 \times 10^7$ m^3/mol and $K_{NO_2} = 0.44 \times 10^7$ m^3/mol).

It is worth to mention that the values for the ratio $(k_5 K_{NO_2}/k_3 K_{NO})$ obtained in both approximate and complete models are nearly equal. In addition, the predicted ratio between the NO_2 and NO concentration at the reactor outlet by the complete model is approximately constant (NO_2 is about the (9.12 ± 0.17)% of NO at the reactor outlet) and this value is also in very good agreement with the ratio obtained in the approximate model. Nevertheless, it is important to notice that the values of $k_5 K_{NO_2}$ and $k_3 K_{NO}$ provided by both models differ by a factor of nearly two. This is certainly a consequence of the simplifications and parameters rearrangement made in the approximate model.

Table 4
Linear regression results from the approximate solution of the differential equation of NO_2 concentration in function of NO concentration.

Parameter	Value	Standard error	Lower 95% confidence interval	Upper 95% confidence interval
$\frac{1}{(k'_5 K'_{NO_2}/k'_3 K'_{NO})-1}$	0.084	0.008	0.066	0.102
$\frac{k'_5 K'_{NO_2}}{k'_3 K'_{NO}}$	12.90	1.27	10.14	15.67
k'_3 (mol dm^{-2} min^{-1})	0.239×10^{-7}	0.029×10^{-7}	0.177×10^{-7}	0.302×10^{-7}
K'_{NO} (dm^3 mol^{-1})	12.44×10^7	2.76×10^7	6.46×10^7	18.43×10^7
$k'_5 K'_{NO_2}$ (dm min^{-1})	38.41	7.68	21.72	55.09
R^2	0.879			
N (*)	14			

(*) Number of data.

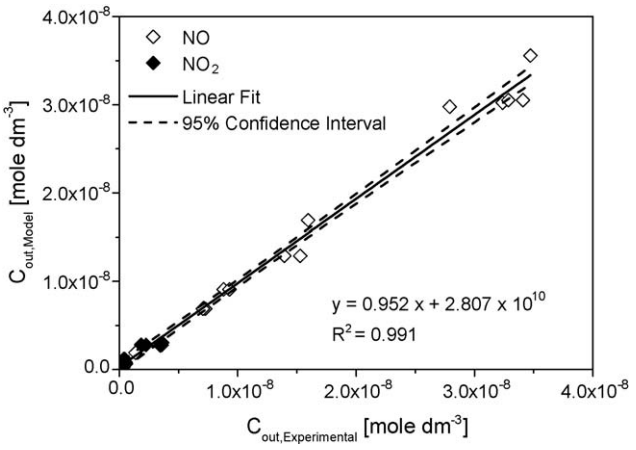

Fig. 8. NO and NO_2 outlet concentration predicted by the model employing the estimated kinetic parameters vs. the experimental data.

Fig. 8 shows the complete model predictions corresponding to the NO and NO_2 outlet concentration in function of the NO and NO_2 experimental data obtained in the photoreactor. These last values should be over a line with a slope close to 1 and an ordinate intercept equal to 0, as Fig. 8 and Table 6 show. In all cases, the model predictions show good agreement with the experimental results. Besides, the complete model predictions and the experimental values of the outlet concentration of NO and NO_2 can be compared in Table 7.

Despite of the accuracy and suitability of the complete model in predicting the experimental results, the approximate model can be easily and quickly applied to provide a rough but valuable estimation of the kinetic parameters involved. For instance, this model could be very useful to practically evaluate the air purifying performance of photocatalytic construction materials using ISO 22197-1 standard [26].

4. Experimental results vs. modelling

It is possible to analyze the effect of different operating variables on the system by resorting the estimated kinetic parameters from the complete model. This analysis can include a comparison between simulated values obtained with the model and experimental measurements.

Fig. 9 shows the model predictions and the experimental data corresponding to the NO and NO_2 outlet concentration in function of the NO inlet concentration to the reactor for two different flow rates. When the inlet concentration of NO increases, both NO and NO_2 outlet concentration rise as well. However, as expected, decreasing the initial concentration of the pollutant the final conversion of the reacting system increases (see Table 1).

The effect of the flow rate is possible to analyze comparing Fig. 9(a) and (b). When the flow rate is increased the resident time in the reactor decreases. Therefore, for low flow rates a larger conversion of the pollutant is observed.

If the reactor height is varied, no changes in the outlet concentration are observed, as Fig. 10 shows for NO and NO_2 concentration. The explanation of this behavior can be found considering the height effect over the air velocity or resident time and over the total reactor volume. On the one hand, with higher reactor height lower air velocity and longer resident time are obtained resulting in a higher conversion. On the other hand, the reactor volume is larger and for the same photocatalytic active surface a smaller degradation conversion is achieved due to the products dissolution in the gas phase. These parameters (resident time and reactor volume) have opposite effects over the final conversion, resulting in a constant outlet concentration for different reactor heights.

Table 6
Linear regression results of the concentration predicted by the complete model vs. the experimental data.

Parameter	Value	Standard error	Lower 95% confidence interval	Upper 95% confidence interval
Slope	0.952	0.017	0.917	0.988
Ordinate intercept	2.81×10^{-10}	2.56×10^{-10}	-2.45×10^{-10}	8.06×10^{-10}
R^2	0.991			
N (*)	29			

(*) Number of data.

Table 7
Experimental and complete model results of the NO_x photocatalytic degradation.

Experiment #	$C_{NO,in} \times 10^8$ mol dm^{-3}	$C_{NO,out} \times 10^8$ mol dm^{-3}	$C_{NO,out,\ Model} \times 10^8$ mol dm^{-3}	$C_{NO_2,in} \times 10^8$ mol dm^{-3}	$C_{NO_2,out} \times 10^8$ mol dm^{-3}	$C_{NO_2,out,Model} \times 10^8$ mol dm^{-3}
1	0.430	0.136	0.190	0.008	0.024	0.018
2	1.357	0.712	0.696	0.015	0.028	0.064
3	1.346	0.725	0.690	0.016	0.040	0.064
4	1.346	0.705	0.690	0.024	0.055	0.064
5	2.257	1.392	1.290	0.019	0.037	0.119
6	2.257	1.527	1.290	0.039	0.044	0.119
7	4.419	2.789	2.978	0.066	0.344	0.272
8	4.472	3.237	3.023	0.081	0.358	0.276
9	4.506	3.287	3.052	0.072	0.187	0.278
10	4.507	3.410	3.052	0.063	0.225	0.278
11	0.454	0.184	0.281	0.010	0.035	0.026
12	1.342	0.882	0.910	0.020	0.054	0.083
13	1.342	0.930	0.911	0.023	0.039	0.083
14	2.242	1.594	1.690	–	–	0.150
15	4.458	3.472	3.558	0.087	0.362	0.306

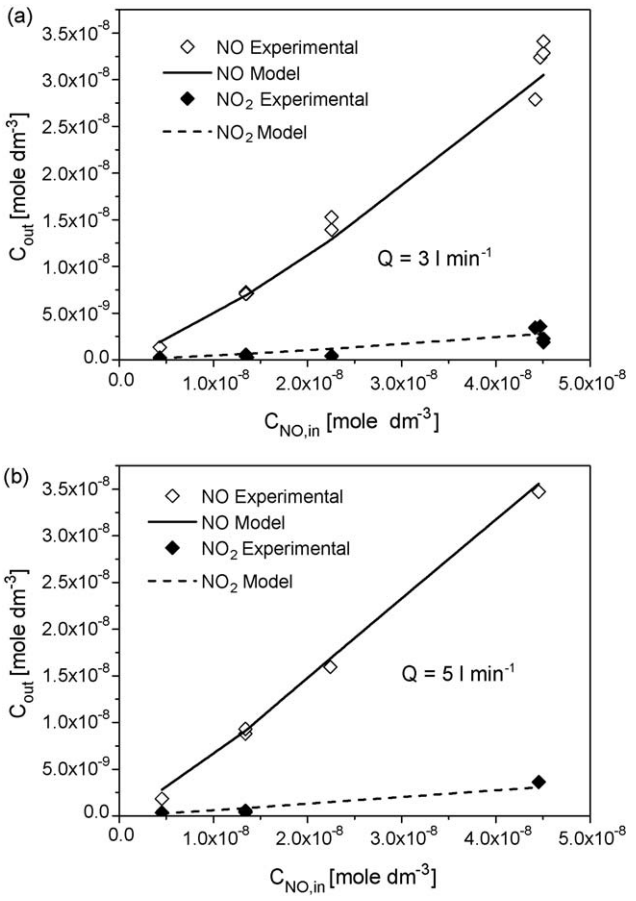

Fig. 9. Model predictions vs. experimental data. NO and NO_2 outlet concentration in function of the NO inlet concentration. (a) $Q = 3\ l\ min^{-1}$. (b) $Q = 5\ l\ min^{-1}$.

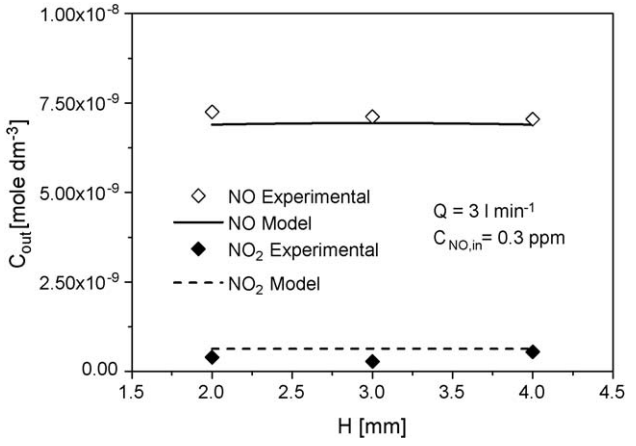

Fig. 10. Model predictions vs. experimental data. Effect of the reactor height over the degradation rate. $Q = 3\ l\ min^{-1}$. $C_{NO,in} = 0.3$ ppm.

5. Conclusion

In the present work, a kinetic study of the photocatalytic degradation of nitrogen oxides was conducted. A heterogeneous kinetic expression for the NO degradation and for the NO_2 appearance/disappearance was proposed. Several experiments were carried out according a suitable ISO standard for photocatalytic materials assessment employing only NO as the contaminant. Different operating conditions were selected to carry out the experiments (varying NO inlet concentration, reactor height and flow rate) while relative humidity, temperature and irradiance remained constant during the experiments (50%, 20 °C and $10\ W\ m^{-2}$). Employing these experimental data and the kinetic expressions, the kinetic parameters for NO and NO_2 were estimated for an approximated and for a complete solution of the governing equations in the reactor and they were compared. In all cases, a very good correlation between the experimental data and the computer simulations with the estimated kinetic parameters was obtained, allowing to explain the degradation of NO and the apparition of NO_2 in this kind of system. A fixed NO_2/NO ratio of about 0.084–0.091 was found with both the approximate and the complete models.

Acknowledgements

The authors wish to express their thanks to the following sponsors of the research group: Bouwdienst Rijkswaterstaat, Rokramix, Betoncentrale Twenthe, Graniet-Import Benelux, Kijlstra Beton Mortel, Struyk Verwo Groep, Hülskens, Insulinde, Dusseldorp Groep, Eerland Recycling, ENCI, Provincie Overijssel, Rijkswaterstaat Directie Zeeland, A&G maasvlakte, BTE, Alvon Bouwsystemen, V.d. Bosch Beton, Twee "R" Recycling and GMB (chronological order of joining).

References

[1] M.R. Hoffmann, S.T. Martin, W. Choi, D.W. Bahnemann, Chem. Rev. 95 (1995) 69–96.
[2] R.W. Matthews, Water Res. 20 (5) (1986) 569–578.
[3] R.W. Matthews, in: E. Pelizzetti, M. Schiavello (Eds.), Photochemical Conversion and Storage of Solar Energy, Kluwer Academic Publishers, Dordrecht, 1991, pp. 427–449.
[4] D.F. Ollis, E. Pellizzetti, Environ. Sci. Technol. 25 (9) (1991) 1523–1529.
[5] EU – The Council of the European Union, Council Directive 1999/30/EC – Relating to Limit Values for Sulphur Dioxide, Nitrogen Dioxide and Oxides of Nitrogen, Particulate Matter and Lead in Ambient Air, 1999.
[6] J. Zhang, Y. Hu, M. Matsuoka, H. Yamashita, M. Minagawa, H. Hidaka, M. Anpo, J. Phys. Chem. B 105 (2001) 8395–8398.
[7] T. Ibusuki, K. Takeuchi, J. Mol. Catal. 88 (1994) 93–102.
[8] K. Hashimoto, K. Wasada, M. Osaki, E. Shono, K. Adachi, N. Toukai, H. Kominami, Y. Kera, Appl. Catal. B: Environ. 30 (2001) 429–436.
[9] J.S. Dalton, P.A. Janes, N.G. Jones, J.A. Nicholson, K.R. Hallam, G.C. Allen, Environ. Pollut. 120 (2002) 415–422.
[10] H. Ichiura, T. Kitaoka, H. Tanaka, Chemosphere 51 (2003) 855–860.
[11] S. Devahasdin, C. Fan, J.K. Li, D.H. Chen, J. Photochem. Photobiol. A: Chem. 156 (2003) 161–170.
[12] Y.M. Lin, Y.H. Tseng, J.H. Huang, C.C. Chao, C.C. Chen, I. Wang, Environ. Sci. Technol. 40 (2006) 1616–1621.
[13] B.N. Shelimov, N.N. Tolkachev, O.P. Tkachenko, G.N. Baeva, K.V. Klementiev, A.Y. Stakheev, V.B. Kazansky, J. Photochem. Photobiol. A: Chem. 195 (2008) 81–88.
[14] A. Fujishima, K. Hashimoto, T. Watanabe, TiO_2 Photocatalysis Fundaments and Applications, BKC, Inc., Chiyoda-ku, Tokyo, 1999.
[15] M. Lackhoff, X. Prieto, N. Nestle, F. Dehnb, R. Niessner, Appl. Catal. B: Environ. 43 (2003) 205–216.
[16] C.S. Poon, E. Cheung, Const. Build. Mater. 21 (2007) 1746–1753.
[17] H. Wang, Z. Wu, W. Zhao, B. Guan, Chemosphere 66 (2007) 185–190.
[18] T. Maggos, G.J. Bartzis, M. Liakou, C. Gobin, J. Hazard. Mater. 146 (2007) 668–673.
[19] T. Maggos, J.G. Bartzis, P. Leva, D. Kotzias, Appl. Phys. A 89 (2007) 81–84.
[20] T. Maggos, A. Plassais, J.G. Bartzis, C. Vasilakos, N. Moussiopoulos, L. Bonafous, Environ. Monit. Assess. 136 (2008) 35–44.
[21] Y. Murata, H. Tawara, H. Obata, K. Murata, NO_x-Cleaning Paving Block, EP-patent 0786283 A1, Mitsubishi Materials Corporation, Japan, 1997.
[22] C. Terruzzi, A pavement with Photocatalytic Effect, EP1609910, Global Engineering and Trade, Italy, 2005.
[23] R. Cucitore, S. Cangiano, L. Cassar, High Durability Photocatalytic Paving for reducing Urban Polluting Agents, WO2006000565, Italcementi SPA, Italy, 2006.
[24] L. Cassar, R. Cucitore, C. Pepe, Cement-Based Paving Blocks for Photocatalytic Paving for the Abatement of Urban Pollutants, EP-patent 1601626, Italcementi SPA, Italy, 2005.
[25] R. Alfani, New precast cementitious Products with Photocatalytic Activity, WO2008017934, Italcementi SPA, Italy, 2008.
[26] ISO 22197-1, Fine ceramics (advanced ceramics, advanced technical ceramics) – Test method for air purification performance of semiconducting photocatalytic materials – Part 1: Removal of nitric oxide, first ed., 2007.
[27] G. Hüsken, M. Hunger, H.J.H. Brouwers, in: P. Baglioni, L. Cassar (Eds.), Proceedings International RILEM Symposium on Photocatalysis, Environment and Construction Materials-TDP, RILEM Publications, Bagneux, 2007, pp. 147–154.
[28] M. Hunger, H.J.H. Brouwers, Cem. Conc. Res. 40 (2010) 313–320.

[29] D.F. Ollis, in: D.F. Ollis, H. Al-Ekabi (Eds.), Photocatalytic Purification and Treatment of Water and Air, Elsevier Science, Amsterdam, 1993, pp. 481–494.
[30] Y. Dong, Z. Bai, R. Liu, T. Zhu, Atmos. Environ. 41 (15) (2007) 3182–3192.
[31] J. Zhao, X.D. Yang, Build. Environ. 38 (5) (2003) 645–654.
[32] M.I. Cabrera, A.C. Negro, O.M. Alfano, A.E. Cassano, J. Catal. 172 (1997) 380–390.
[33] O. Levenspiel, Chemical Reaction Engineering, Willey, New York, 1999.
[34] M.F.J. Dijkstra, H.J. Panneman, J.G.M. Winkelman, J.J. Kelly, A.A.C.M. Beenackers, Chem. Eng. Sci. 57 (2002) 4895–4907.
[35] G.E. Imoberdorf, H.A. Irazoqui, A.E. Cassano, O.M. Alfano, Ind. Eng. Chem. Res. 44 (2005) 6075–6085.